Inorganic Chemistry

Article

pubs.acs.org/IC

Orbital Origins of Helices and Magic Electron Counts in the Nowotny Chimney Ladders: the 18 − *n* Rule and a Path to Incommensurability

Vincent J. Yannello and Daniel C. Fredrickson*

Department of Chemistry, University of Wisconsin—Madison, 1101 University Avenue, Madison, Wisconsin 53706, United States

Supporting Information

ABSTRACT: Valence electron count is one of the key factors influencing the stability and structure of metals and alloys. However, unlike in molecular compounds, the origins of the preferred electron counts of many metallic phases remain largely mysterious. Perhaps the clearest-cut of such electron counting rules is exhibited by the Nowotny chimney ladder (NCL) phases, compounds remarkable for their helical structural motifs in which transition metal (T) helices serve as channels for a second set of helices formed from main group (E) elements. These phases exhibit density of states pseudogaps or band gaps, and thus special stability and useful physical properties, when their valence electron count corresponds to 14 electrons per T atom. In this Article, we illustrate, using DFT-calibrated Hückel calculations and the reversed approximation Molecular Orbital analysis, that the 14-electron rule of the NCLs is, in fact, a specific instance of an 18 − *n* rule emerging for T−E intermetallics, where *n* is the number of E-supported T−T bonds per T atom. The structural flexibility of the NCL series arises from the role of the E atoms as supports for these T−T bonds, which simply requires the E atoms to be as uniformly distributed within the T sublattice as possible. This picture offers a strategy for identifying other intermetallic structures that may be amenable to incommensurability between T and E sublattices.

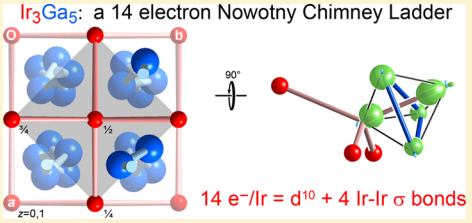

1. INTRODUCTION

Since their discovery in the 1960s, the Nowotny chimney ladder (NCL) phases have been a focal point of both amazement and new developments in the area of solid-state materials. As their structures were determined in systems combining transition metal (T) and main group (E) elements, they were found to be simultaneously complex and elegant,[1−14] as is shown for three examples in Figure 1: $RuGa_2$,[15−17] Ru_2Sn_3,[11] and Ir_3Ga_5.[7] The T atoms (generally from groups 4−9) adopt the flattened diamond network of the β-Sn structure, whose square channels trace out 4-fold helices. Inside these channels, the E atoms (from groups 13−15) form a separate set of helices (blue), whose repeat period changes with the stoichiometry of the phase. The ability of the E helices to adjust to an almost continuous series of T:E ratios made the NCLs one of the first instances of infinitely adaptive structures[18,19] and composite crystals modeled in 3 + 1D space.[20−22] Their structural and electronic characteristics have also led to the NCLs being explored for thermoelectric properties and topological insulating effects.[23−27]

Underlying these intriguing geometrical motifs and physical properties is one of the clearest-cut electron counting rules in intermetallic phases. The T:E ratios of the NCLs are tuned, often quite closely, so that the total number of valence electrons per T atom is 14 (when T is a late transition metal from group 7 or higher).[19,28,29] For example, in Ru_2Sn_3, each Ru atom brings 8 valence electrons to the structure, while each Sn contributes 4, so that the electron count per Ru atom is $(2 \times 8 + 3 \times 4)/2 = 14$, and the same number is obtained by applying similar arithmetic to the other phases of Figure 1.

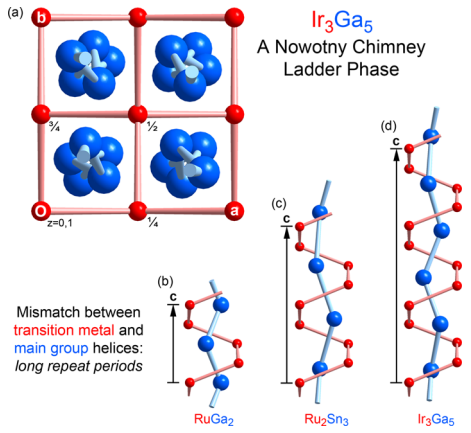

Figure 1. Structural features of the NCL phases. (a) View down *c* of the Ir_3Ga_5 structure showing the helix-within-a-helix motif of these compounds. The numbers in black give the heights of the Ir atoms in fractions of the helical repeat of the transition metal sublattice. (b− d) The *c* repeat periods of (b) $RuGa_2$, (c) Ru_2Sn_3, and (d) Ir_3Ga_5 are determined by the number of turns of the transition metal helix necessary for reaching an equivalent point in the main group helix: one for $RuGa_2$, two for Ru_2Sn_3, and three for Ir_3Ga_5.

For this reason, the NCLs have been the subject of a number of theoretical studies, which have consistently connected the special stability of the 14-electron count to band gaps or pseudogaps at the Fermi energy (E_F).[30−36] However, a full

Received: July 17, 2014
Published: September 12, 2014

   dx.doi.org/10.1021/ic501723n | *Inorg. Chem.* 2014, 53, 10627−10631

account of the origin of gaps at this particular electronic count across the series is still needed. The persistence of this mystery—despite significant advances in computational power, methodology, and tools for bonding analysis since the first articulation of the 14-electron rule—highlights a fundamental challenge for theory in intermetallics. These phases contain a wide variety of competing bonding types, whose accurate modeling requires high-level calculations. Yet, electron counting rules are generally based on sequences of energy levels with different numbers of nodes, e.g., simple molecular orbital (MO) diagrams, which become increasingly difficult to identify as calculations become more advanced.

In the course of our recent investigations into T−E phases,[37−39] we have developed a theoretical approach to resolving this paradoxical need for both accuracy and simplicity in the analysis of intermetallics: the reversed approximation MO (raMO) method.[39] In this approach, we analyze the electronic structure of a compound by using its occupied wave functions as an approximate basis set for solving the Schrödinger equations for simple model systems whose MO diagrams are hypothesized to feature in the bonding of the phase. The resulting eigenvectors map the electronic structure of the full compound onto the proposed MO scheme.

Our initial successes with the raMO method encouraged us to see what this approach can tell us about the orbital interactions underlying the 14-electron rule of the NCLs. In this Article, we illustrate how raMO analyses on a series of these compounds reveal the orbital origins of both the 14-electron rule and the remarkable helical features of the NCLs. Perhaps more importantly, the resulting bonding picture also anticipates a general electron counting scheme for T−E intermetallics and offers a synthetic strategy for developing new series of incommensurately ordered phases.

2. EXPERIMENTAL SECTION

Electronic structure calculations were carried out on the crystal structures of $RuGa_2$, Ru_2Sn_3, and Ir_3Ga_5 using local-density approximation density functional theory (LDA-DFT) with the Vienna Ab initio Simulation Package.[40,41] The structures of the phases were optimized using a two-step procedure: first the atomic positions were relaxed in a fixed unit cell, and then all structural parameters were released. Single-point calculations were carried out on the resulting equilibrium geometries to obtain band energies and density of states (DOS) curves. All LDA-DFT calculations were performed in the high-precision mode and employed the ultrasoft pseudopotentials provided with the package.[42] Additional computational details, including the energy cutoffs, *k*-point meshes, and optimized geometries, are provided in the Supporting Information.

The LDA-DFT results were used as the basis for the parametrization of simple Hückel models using the program *eHtuner*,[43] which invokes *YAeHMOP* for the actual Hückel calculations.[44] Tables of the optimized Hückel parameters and comparisons between the LDA-DFT and Hückel results are given in the Supporting Information. For the raMO analyses, simple Hückel calculations were performed with *YAeHMOP* on a 2 × 2 × 2 supercell of the conventional cells of the phases to map several high-symmetry *k* points to the Γ point. The Hamiltonian matrix at the Γ point was then extracted and imported in *Matlab*, where raMO analyses were executed using custom-made functions.

3. RESULTS AND DISCUSSION

We began our analyses of the NCLs by developing DFT-calibrated Hückel models for the 14-electron compounds shown in Figure 1. This was accomplished by first performing LDA-DFT calculations on the compounds and then using the output for each phase as reference data for optimization of the Hückel parameters (see the Experimental Section). For the NCLs, Hückel parameters were obtainable that reproduce the DFT band energies to a root-mean-square deviation of less than 0.15 eV (for all bands up to 1 eV above the E_F). These models can then be considered as a translation of the DFT electronic structure into an effective orbital-based picture.

The DOS distributions obtained from these Hückel models of the three phases are presented in Figure 2. All three curves

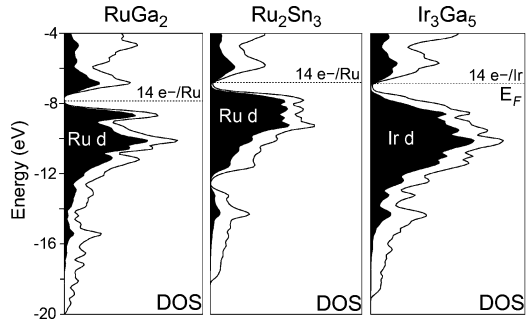

Figure 2. Electronic DOS curves for DFT-calibrated Hückel models of three NCLs. The contributions to the DOS from the transition metal d orbitals are shaded.

have a similar form, with a narrow parabolic distribution of E sp-rich states at low energies, followed by a dense block of T d states (shaded). In each case, the top of the densest part of the T d states coincides with the E_F and a deep DOS minimum that reaffirms the special stability of the 14-electron count.

With these DFT-calibrated Hückel models in hand, we are ready to begin using the raMO method to break down the electronic structure of the NCLs into simple MO diagrams. Let us start with $RuGa_2$ as it crystallizes in the parent structure of the NCL series: the $TiSi_2$ type (Figure 3a).[15−17] Here, the repeat periods of the T and E helices are perfectly in-sync, and only one symmetry-distinct site occurs for the Ru and Ga atoms.

The first step in a raMO analysis is to propose a local MO diagram that is expected to be relevant to the full electronic structure. Given the importance of Ru atoms to the electron counting, the energy level diagram of the Ru valence atomic orbitals provides an excellent first guess. To pursue this, we construct a model Hamiltonian operator in which the Ru's nine valence orbitals (5s, 5p, 4d) are eigenfunctions. Next, we calculate matrix elements of this model Hamiltonian using the occupied wave functions of $RuGa_2$ as our basis. Diagonalization of the resulting matrix yields nine functions, which represent the best approximations to the target functions that can be constructed from linear combinations of $RuGa_2$'s occupied wave functions.

These raMO functions are plotted in the context of the Ru coordination environment in Figure 3c. This coordination environment contains 10 Ga atoms: six in a hexagon surrounding the Ru at distances of 2.73 or 2.74 Å and four closer Ga neighbors (2.57 Å from the central Ru) in pairs above and below this plane.[16] In addition, there are four Ru neighbors arranged in a tetrahedron flattened along *c* at a longer distance of 3.21 Å.

For each raMO function in Figure 3c, a different member of Ru's complement of nine valence atomic orbitals appears at the center of this coordination polyhedron. In each case, these Ru

dx.doi.org/10.1021/ic501723n | *Inorg. Chem.* 2014, 53, 10627−10631

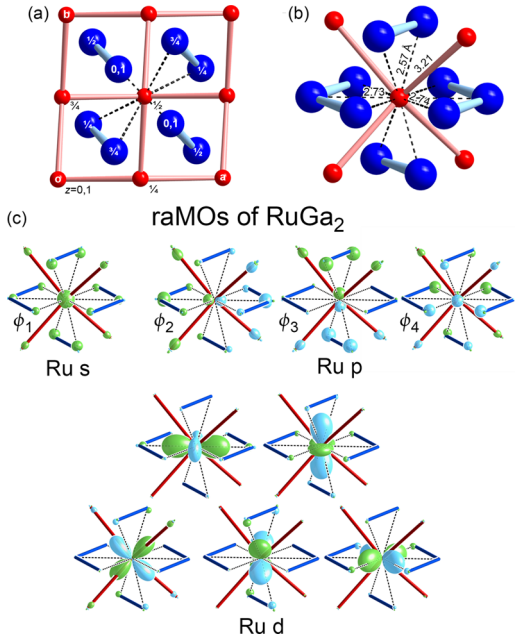

Figure 3. raMO analysis of $RuGa_2$ using the Ru 5s, 5p, and 4d orbitals as target states. (a) Crystal structure of $RuGa_2$ (shown in a nonstandard *I*-centered setting for comparison with the other NCLs). (b) The Ru coordination environment. (c) raMOs generated using the Ru valence atomic orbitals as target states.

orbitals are complemented by in-phase contributions from the surrounding Ga atoms, indicating the strong role of Ru−Ga interactions in the bonding of this phase. Stronger contributions from the central Ru are seen for the Ru 4d functions than for the Ru 5s or 5p ones. This stems from the lower energy of the 4d orbitals and their higher population by electrons in the full electronic structure. The 5s and 5p functions show larger orbital character on the Ru atom's neighbors, suggesting that their electrons are more delocalized away from the Ru center. Each of these functions, however, is well-localized to the first coordination shell of the Ru atom and represents an electron pair in a function with the same nodal properties as the original Ru atomic orbital.

Our ability to assign an electron pair to each of the nine functions in Figure 3c suggests that the central Ru atom has 18 electrons associated with it, which recalls the electron configurations of 18-electron organometallic or coordination compounds (where the 18 electrons assigned to a T center are in orbitals of varying degrees of polarization between the T atom and its surrounding atoms, just as in this case). How is it then that the preferred electron count occurs at 14 rather than 18 electrons/Ru? The answer to this question lies in the observation that the raMOs of the Ru atom exhibit bonding contributions from its neighboring Ru atoms. This is most easily seen in the raMOs for the 5s and 5p orbitals, where hybrid orbitals on the Ru neighbors point toward the central atom in symmetry-adapted linear combinations reminiscent of the $a_1 + t_2$ irreducible representations (IRs) of the ligand σ orbitals in a tetrahedral complex. The presence of this Ru−Ru bonding indicates that the electron configurations of the Ru atoms are not independent of each other but instead share electrons. This, in turn, is expected to lower the total number of electrons necessary to reach closed shells.

The similarity of these functions to the IRs of a tetrahedral field offers a simple way of obtaining a clearer view of the electron sharing between Ru atoms. In Figure 4, we take linear combinations of the one s-based and three p-based functions to

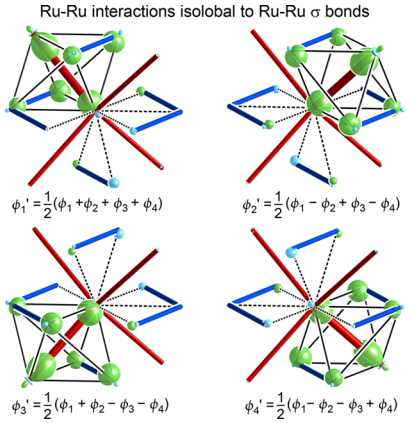

Figure 4. Localized linear combinations of the $RuGa_2$ raMOs approximating the Ru 5s and 5p orbitals (ϕ_1 through ϕ_4 in Figure 3). Each function corresponds to an electron pair in a multicenter interaction isolobal to a Ru−Ru σ bond.

create sp^3 hybrids pointing to the corners of a tetrahedron. In each case, a lobe is obtained pointing from the central Ru toward one of its Ru neighbors. This is met on the other side of the Ru−Ru contact by another large hybrid orbital pointing into the bond. The interaction is also strengthened by bonding contributions from four bridging Ga atoms that trace out a square around the Ru−Ru contact. Overall, each of the localized functions has the form of a multicenter bond spread out over the corners of a $RuGa_4Ru$ octahedron. In terms of their symmetry properties, these functions are isolobal to simple two-center two-electron Ru−Ru σ bonds. In terms of electron counting, we can then consider there to be a covalently shared electron pair at each Ru−Ru contact.

Because these functions play the same role in terms of electron counting and share the symmetry properties as a classical T−T σ bond, we find it convenient to refer to them as "E-supported T−T bonds" or simply "T−T bonds." While using such terms, however, one should recognize that these bonding functions have multicenter character in which the major stabilizing interactions are likely between the T atoms and E bridges rather than through-space T−T overlap.

With the identification of these shared electron pairs, the origin of the 14-electron rule comes into focus. For a Ru atom without any Ru neighbors, we would expect a closed-shell electron configuration to occur at 18 electrons, so that an electron pair is associated with each of its 5s, 5p, and 4d orbitals. If we begin to introduce shared electron pairs between Ru atoms, the number of electrons needed per Ru atom is reduced. For each Ru−Ru bond, the participating Ru atoms need one fewer electron for a filled shell. For *n* Ru−Ru bonds per Ru atom, the preferred electron count would then be $18 - n$ electrons/Ru. In $RuGa_2$, where each Ru atom is surrounded by four Ru neighbors, the ideal electron count is simply $18 - 4 = 14$.

In this way, we seem to have accounted for all of the valence electrons in $RuGa_2$ by considering just Ru-centered raMO functions. This conclusion is supported by a raMO analysis in which we use all of the Ru valence orbitals in the crystal structure as target functions. Such a procedure results in no remainder states (functions orthogonal to the model

dx.doi.org/10.1021/ic501723n | *Inorg. Chem.* 2014, 53, 10627−10631

Hamiltonian), indicating that the Ru-centered raMOs are able to account for the full electronic structure of $RuGa_2$. As such, the number of electrons that can be accommodated by the structure is determined by the Ru−Ru contacts within the Ru sublattice. The primary role of Ga is simply to participate in Ru−Ga bonding and to stabilize the Ru−Ru bonds through bridging interactions.

From this point of view, we begin to see how helical and incommensurate structures can arise in the NCL family. Substituting, say, the Ru of $RuGa_2$ with Ir or the Ga with Sn would lead to electron counts in excess of 14 electrons/T if we were to keep the 1:2 stoichiometry. $IrGa_2$ would have 15 electrons/Ir, while $RuSn_2$ would have 16 electrons/Ru. The removal of main group atoms from the structure could allow for the number of electrons per T atom to be reduced, without affecting the overall architecture of the T−T bonds. For $IrGa_2$, the excess of one electron could be corrected through the deletion of $^1/_3$ of a Ga atom per Ir, leading to the stoichiometry $IrGa_{1.667} = Ir_3Ga_5$. Likewise, for $RuSn_2$, the extra two electrons could be removed by taking out $^1/_2$ of a Sn atom per Ru, to give $RuSn_{1.5} = Ru_2Sn_3$. These are, of course, the experimentally observed stoichiometries of the Ir−Ga and Ru−Sn NCLs.

This hypothesis can be simply tested by performing raMO analyses on Ru_2Sn_3 and Ir_3Ga_5. The raMOs generated using the T valence atomic orbitals as target eigenstates show a close correspondence to those of $RuGa_2$, as can be seen in the Supporting Information. Most importantly, the s- and p-centered raMOs can be similarly localized to create bonding functions along each of the T−T contacts. These localized T−T functions are shown alongside those of $RuGa_2$ in Figure 5.

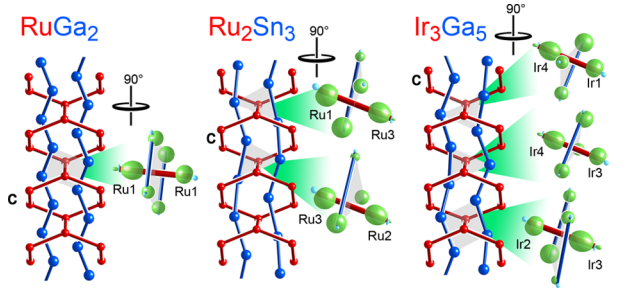

Figure 5. Isolobality of T−T interactions across the NCL series. Localized T−T σ functions derived from the T s and p raMOs are shown for each symmetry-distinct T−T contact in $RuGa_2$, Ru_2Sn_3, and Ir_3Ga_5. For each phase, the T atoms engage in four such interactions isolobal to a classical T−T σ bond, making only 18 − 4 = 14 electrons/T needed to complete filled 18-electron configurations.

Just as in $RuGa_2$, the T−T functions of Ru_2Sn_3 and Ir_3Ga_5 exhibit the same symmetry properties as a standard two-center two-electron T−T bond but are delocalized through interactions with bridging E atoms. The involvement of these bridging interactions may explain why no electron localization maxima were found along the T−T contacts in an earlier analysis of the NCL $ZrBi_{1.62}$:[14] stronger overlap of the T−E interactions versus the through-space T−T ones could lead to the bonding in the T−T σ functions being more concentrated on the bridges.

The major differences in the raMO results of the phases arise in how the T−T bonds are supported by E atoms. For $RuGa_2$, the bonds involve bridging E atoms arranged in a square around the T−T contact. After E atoms are deleted to arrive at the Ru_2Sn_3 or Ir_3Ga_5 stoichiometries, there are no longer enough E atoms for such squares to be placed at every T−T interaction. Triangles of bridging atoms occur instead for two of the three symmetry-distinct T−T contacts in Ir_3Ga_5 and for all of these contacts in Ru_2Sn_3. The resilience of the 14 electrons/T DOS minima across this series indicates that triangles of bridging E atoms are still sufficient for stabilizing electron pairs at the T−T contacts.

4. CONCLUSIONS

In summary, the 14-electron rule of the NCL phase has a simple orbital origin. As in organometallic and coordination complexes, the T atoms of the NCLs strive to achieve filled 18-electron configurations. This is accomplished through the covalent sharing of electron pairs at four T−T contacts around each T atom. Filled 18-electron configurations then only require 18 − 4 = 14 electrons per T atom. In this way, the NCLs can be incorporated into a more general electron counting rule that is emerging in our investigations of T−E intermetallics: closed-shell electron configurations can be associated with 18 − n electrons per T atom, where n is the average number of T−T contacts, with additional electrons sometimes belonging to E−E bonds that do not interact with the T atoms. The growing list of compounds adhering to this electron counting scheme includes the 18-electron half-Heusler phases,[45,46] $NiSi_2$,[37] $Fe_8Al_{17.4}Si_{7.6}$,[37] and $CrGa_4$[39] (all with n = 0), as well as Ir_3Sn_7 (n = 1) and Os_3Sn_7 (n = 2).[39]

With this bonding scheme in place, the characteristic structural motifs of the NCLs can be directly related to electronics. The arrangement of the T atoms into a 4-connected network provides the foundation for the full electronic structure of the phase. Geometrical perturbations to this sublattice would threaten to strain its T−T interactions and jeopardize the band gap or pseudogap at the 14-electron count. Thus, the T sublattice remains essentially conserved over the whole NCL series. The major role of the E atoms, on the other hand, is to bond to the T atoms and stabilize the T−T bonds. As such, they adopt an arrangement that homogeneously distributes them within the T sublattice: helices that turn inside the T sublattice channels.

This structural dichotomy between a rigid 3D framework and a continuously adjustable supporting sublattice suggests an approach to developing other series of superstructures and incommensurate phases in T−E intermetallics. We begin by identifying simple structure types with similar networks of T−T bonds and determining their ideal electron counts using the 18 − n rule (which could then be confirmed with calculations). Finally syntheses can be performed in which elemental substitutions are introduced to drive E atom vacancies through the need to maintain an 18 − n electron count. A direction for future research is identifying such candidate parent structures and synthetically exploring their potential as gateways to new intermetallic superstructures.

■ ASSOCIATED CONTENT

Supporting Information

Details concerning the computational procedures, tables of DFT-calibrated Hückel parameters, and comparisons of band structures for $RuGa_2$, Ru_2Sn_3, and Ir_3Ga_5 from LDA-DFT and best-fit Hückel models. This material is available free of charge via the Internet at http://pubs.acs.org.

dx.doi.org/10.1021/ic501723n | Inorg. Chem. 2014, 53, 10627−10631

AUTHOR INFORMATION

Corresponding Author

*E-mail: danny@chem.wisc.edu.

Notes

The authors declare no competing financial interest.

ACKNOWLEDGMENTS

We thank Joshua Engelkemier, Yiming Guo, and Brandon Kilduff, as well as Drs. Amelia Hadler and Veronica Berns, for performing raMO analyses on related systems as part of our group's survey of T−E intermetallics. We also gratefully acknowledge financial support of the Wisconsin Alumni Research Foundation.

REFERENCES

(1) Schwomma, O.; Nowotny, H.; Wittmann, A. *Monatsh. Chem.* **1964**, *95*, 1538−1543.
(2) Schwomma, O.; Preisinger, A.; Nowotny, H.; Wittmann, A. *Monatsh. Chem.* **1964**, *95*, 1527−1537.
(3) Völlenkle, H.; Wittmann, A.; Nowotny, H. *Monatsh. Chem.* **1964**, *95*, 1544−1549.
(4) Flieher, G.; Völlenkle, H.; Nowotny, H. *Monatsh. Chem.* **1967**, *98*, 2173−2179.
(5) Knott, H. W.; Mueller, M. H.; Heaton, L. *Acta Crystallogr.* **1967**, *23*, 549−555.
(6) Völlenkle, H.; Preisinger, A.; Nowotny, H.; Wittmann, A. *Z. Kristallogr.* **1967**, *124*, 9.
(7) Völlenkle, H.; Wittmann, A.; Nowotny, H. *Monatsh. Chem.* **1967**, *98*, 176−183.
(8) Zwilling, G.; Nowotny, H. *Monatsh. Chem.* **1973**, *104*, 668−675.
(9) Israiloff, P.; Völlenkle, H. *Monatsh. Chem.* **1974**, *105*, 1313−1321.
(10) Boller, H. *Monatsh. Chem.* **1974**, *105*, 934−943.
(11) Poutcharovsky, D. J.; Yvon, K.; Parthé, E. *J. Less Common Met.* **1975**, *40*, 139−144.
(12) Kleinke, H. *Inorg. Chem.* **2001**, *40*, 95−100.
(13) Elder, I.; Lee, C.-S.; Kleinke, H. *Inorg. Chem.* **2002**, *41*, 538−545.
(14) Boström, M.; Lind, H.; Lidin, S.; Niewa, R.; Grin, Y. *Solid State Sci.* **2006**, *8*, 1173−1180.
(15) Laves, F.; Wallbaum, H. J. *Z. Kristallogr.* **1939**, *101*, 78.
(16) Jeitschko, W.; Holleck, H.; Nowotny, H.; Benesovsky, F. *Monatsh. Chem.* **1963**, *94*, 838−840.
(17) Jeitschko, W. *Acta Crystallogr., Sect. B* **1977**, *33*, 2347−2348.
(18) Anderson, J. S. *J. Chem. Soc., Dalton Trans.* **1973**, 1107−1115.
(19) Lu, G.; Lee, S.; Lin, J.; You, L.; Sun, J.; Schmidt, J. T. *J. Solid State Chem.* **2002**, *164*, 210−219.
(20) Rohrer, F. E.; Lind, H.; Eriksson, L.; Larsson, A. K.; Lidin, S. *Z. Kristallogr.* **2000**, *215*, 650−660.
(21) Rohrer, F. E.; Lind, H.; Eriksson, L.; Larsson, A. K.; Lidin, S. *Z. Kristallogr.* **2001**, *216*, 190−198.
(22) Sun, J.; Lee, S.; Lin, J. *Chem.—Asian J.* **2007**, *2*, 1204−1229.
(23) Kishida, K.; Ishida, A.; Tanaka, K.; Inui, H. *Mater. Sci. Forum* **2007**, *561−565*, 463−466.
(24) Higgins, J. M.; Schmitt, A. L.; Guzei, I. A.; Jin, S. *J. Am. Chem. Soc.* **2008**, *130*, 16086−16094.
(25) Miyazaki, Y.; Igarashi, D.; Hayashi, K.; Kajitani, T.; Yubuta, K. *Phys. Rev. B* **2008**, *78*, 214104.
(26) Kishida, K.; Ishida, A.; Koyama, T.; Harada, S.; Okamoto, N. L.; Tanaka, K.; Inui, H. *Acta Mater.* **2009**, *57*, 2010−2019.
(27) Gibson, Q. D.; Evtushinsky, D.; Yaresko, A. N.; Zabolotnyy, V. B.; Ali, M. N.; Fuccillo, M. K.; Van den Brink, J.; Buchner, B.; Cava, R. J.; Borisenko, S. V. *Sci. Rep.* **2014**, *4*, 5168.
(28) Jeitschko, W.; Parthé, E. *Acta Crystallogr.* **1967**, *22*, 417−430.
(29) Pearson, W. *Acta Crystallogr., Sect. B* **1970**, *26*, 1044−1046.
(30) Pecheur, P.; Toussaint, G. *MRS Online Proc. Libr.* **1991**, *234*, 157−164.
(31) Pécheur, P.; Toussaint, G.; Kenzari, H.; Malaman, B.; Welter, R. *J. Alloys Compd.* **1997**, *262−263*, 363−365.
(32) Wolf, W.; Bihlmayer, G.; Blügel, S. *Phys. Rev. B* **1997**, *55*, 6918−6926.
(33) Filonov, A. B.; Migas, D. B.; Shaposhnikov, V. L.; Dorozhkin, N. N.; Borisenko, V. E.; Heinrich, A.; Lange, H. *Phys. Rev. B* **1999**, *60*, 16494−16498.
(34) Fredrickson, D. C.; Lee, S.; Hoffmann, R. *Inorg. Chem.* **2004**, *43*, 6159−6167.
(35) Fredrickson, D. C.; Lee, S.; Hoffmann, R.; Lin, J. *Inorg. Chem.* **2004**, *43*, 6151−6158.
(36) Imai, Y.; Watanabe, A. *Intermetallics* **2005**, *13*, 233−241.
(37) Fredrickson, R. T.; Fredrickson, D. C. *Inorg. Chem.* **2012**, *51*, 10341−10349.
(38) Fredrickson, R. T.; Fredrickson, D. C. *Inorg. Chem.* **2013**, *52*, 3178−3189.
(39) Yannello, V. J.; Kilduff, B. J.; Fredrickson, D. C. *Inorg. Chem.* **2014**, *53*, 2730−2741.
(40) Kresse, G.; Furthmüller, J. *Phys. Rev. B* **1996**, *54*, 11169−11186.
(41) Kresse, G.; Furthmüller, J. *Comput. Mater. Sci.* **1996**, *6*, 15−50.
(42) Vanderbilt, D. *Phys. Rev. B* **1990**, *41*, 7892−7895.
(43) Stacey, T. E.; Fredrickson, D. C. *Dalton Trans.* **2012**, *41*, 7801−7813.
(44) Landrum, G. A.; Glassey, W. V. *YAeHMOP: Yet Another extended Hückel Molecular Orbital Package*; YAeHMOP is freely available via the Internet at http://sourceforge.net/projects/yaehmop/. Last accessed: Aug 31, 2014.
(45) Jung, D.; Koo, H. J.; Whangbo, M. H. *THEOCHEM* **2000**, *527*, 113−119.
(46) Kandpal, H. C.; Felser, C.; Seshadri, R. *J. Phys. D: Appl. Phys.* **2006**, *39*, 776−785.